

Cite this: *Phys. Chem. Chem. Phys.*,
2019, 21, 9036

Influence of the average molar mass of poly(*N*-vinylpyrrolidone) on the dimensions and conductivity of silver nanowires†

Luisa Sonntag,^{ab} Franziska Eichler,^a Nelli Weiß,^a Ludwig Bormann,^c Dhriti S. Ghosh,^c Jannick M. Sonntag,^d Rainer Jordan,^{bd} Nikolai Gaponik,^{id}*^{ab} Karl Leo^{bc} and Alexander Eychmüller^{id}^{ab}

We investigate the influence of the average molar mass (M_w) of the capping agent poly(*N*-vinylpyrrolidone) (PVP) on the conductivity of a silver nanowire (AgNW) network. During the polyol process, the chain length of PVP is known to influence the AgNW diameters and lengths. By altering the reaction temperature and time and using PVP of different chain lengths, we synthesized AgNWs with varying diameters, lengths and PVP coverage. The obtained plethora of AgNWs is the basis for conductivity investigations of networks made of AgNWs with a diameter of either 60 nm or 80 nm. The results show a negative influence of long-chain PVP on the conductivity of the subsequent network if 60 nm thick AgNWs are employed. Overall, we obtain well performing AgNW transparent electrodes on glass with $R_s = 24.4 \Omega \text{ sq}^{-1}$ at 85.5% $T_{550\text{nm}}$.

Received 3rd February 2019,
Accepted 13th March 2019

DOI: 10.1039/c9cp00680j

rsc.li/pccp

Introduction

Transparent conductive electrodes (TCEs) fabricated with silver nanowire (AgNW) networks are highly promising candidates for application in optoelectronic devices, such as solar cells, light-emitting-diodes, or touch screens.^{1–6} The AgNW electrodes show comparable sheet resistances (R_s) and transmittances at 550 nm (% T_{550}) to commercially used indium tin oxide (ITO). Since ITO is a ceramic, its brittleness may cause electrode failure after bending or stretching. Also, the ITO vapour deposition process is more expensive than wet-chemical film fabrication. Electrodes consisting of AgNWs on the other hand fulfil the requirements of high conductivity and transparency, while solution-based processing allows low cost and large area deposition techniques.^{7,8} Furthermore, the ductility of silver provides the bend- and stretchability of the AgNW networks on flexible substrates.⁹

Most synthetic approaches rely on the work by Wiley *et al.*, who introduced an one-pot polyol process for producing AgNWs.¹⁰

Here, ethylene glycol (EG) is used as a solvent and a subsequent reducing agent and silver nitrate is used as a silver source. The key condition allowing elongated growth into nanowires is the use of poly(*N*-vinylpyrrolidone) (PVP) as a capping agent, which interacts with the {100}-facet of the silver nanowires leading to preferential deposition of new silver atoms at the {111}-facet.¹¹ Our work is based on an improved one-pot polyol process proposed by Bergin *et al.*, where the addition of $\text{Fe}(\text{NO}_3)_3$ and NaCl reduces oxygen etching and provides a high yield of multi twinned particles (MTPs), which finally grow into the desired AgNWs.¹² Earlier research has shown that the reaction temperature and the reaction time have a major influence on the AgNW diameter D and length L . Here, a higher reaction temperature leads to an increased seed formation resulting in thinner and usually shorter AgNWs.¹²

In the past, several groups have investigated the influence of the mass average molar mass (M_w) of PVP on the AgNW synthesis. Their findings regarding the role of PVP are diverse and based on different synthetic methods. The most agreed requirement to successfully synthesize AgNWs is the use of PVP with critical minimum molar masses which were 10 kDa,¹³ 40 kDa,¹⁴ ~ 50 kDa,^{15–18} or even 1300 kDa.¹⁹ Utilizing PVP of a lower M_w leads to nanorods and nanoparticles of undefined shapes as the main or byproducts and no AgNWs or only in a low yield. Some groups also observed an increase of the nanowire aspect ratio (aspect ratio $A = \text{length/diameter}$) upon increasing the M_w of PVP.^{13–15} Regarding the diameter, controversial outcomes were stated: there was an increase,¹⁸ a decrease,¹⁵ or no change of diameter¹⁶ upon increasing the M_w of PVP. A mixture of PVP with two different M_w s resulted in thinner AgNWs with high

^a Physical Chemistry, Technische Universität Dresden, Bergstraße 66b, 01062 Dresden, Germany. E-mail: nikolai.gaponik@chemie.tu-dresden.de, alexander.eychmueller@chemie.tu-dresden.de

^b Center for Advancing Electronics Dresden (cfaed), Technische Universität Dresden, 01062 Dresden, Germany

^c Dresden Integrated Center for Applied Physics and Photonic Materials (IAPP), Technische Universität Dresden, Nöthnitzer Str. 61, 01187 Dresden, Germany

^d Chair of Macromolecular Chemistry, Faculty of Chemistry and Food Chemistry, School of Science, Technische Universität Dresden, Mommsenstr. 4, 01069 Dresden, Germany

† Electronic supplementary information (ESI) available. See DOI: 10.1039/c9cp00680j



Table 1 overview of the investigations regarding the influence of the average molar mass of PVP on the synthesis and dimensions of AgNWs

Synthetic approach, additives	PVP:Ag	PVP [kDa]	NW		Conclusion regarding PVP	Ref.
			D [nm]	L [μ m]		
Microwave assisted, 198 °C, 3–8 min, H ₂ PtCl ₆ ·6H ₂ (seeds)	5.6:1	10, 40, 360	—	1–20	Length \uparrow and aspect ratio \uparrow with M_w of PVP \uparrow^a	13
Dropwise simultaneously 150 °C, 80 min	1:1	15, 38, 58, 200, 800	100–180	3–10	Yield \uparrow , aspect ratio \uparrow , diameter \downarrow with M_w of PVP \uparrow^a	15
One-pot; FeCl ₃ (dropwise) 130 °C, 5 h	1.2:1	6,10, 30, 40, 65, 1300	—	—	Yield \uparrow , aspect ratio \uparrow with M_w of PVP \uparrow^a	14
One-pot, FeCl ₃ 140 °C, 50 min	1.4:1	55, 360, 1300	25–160	5–50	A mixture of PVP55 and PVP360 (1:2) results in thin wires	20
One-pot, NaCl 185 °C, 20 min	3:1 (was varied)	8, 29, 40, 1300	90–300	1–6	Adsorption and the steric effect of PVP discussed ^a	19
One-pot; NaCl, NaBr 170 °C, 1 min	1.9:1	55, 130	20	40	No influence of the M_w of PVP on diameter ^a	16
Hydrothermal; 160 °C, 3 h, CuCl ₂ ·2H ₂ O (dropwise)	1.5:1 (was varied)	10, 40, 58, 360	47–235	6–70	A mixture of PVP results in thin wires ^a	17
One-pot; 160 °C, 1 h dropwise simultaneously	3:1 (was varied)	10, 55, 360	102–135	20–25	Diameter \uparrow , length \downarrow with M_w of PVP \uparrow^a	18
One-pot; Fe(NO ₃) ₃ , NaCl 140 °C, 2 h	1.5:1	10, 40, 55, 360, 1300	33–262	1–42	Length \uparrow , aspect ratio \uparrow with M_w of PVP \uparrow^a	Current work

^a State critical minimum M_w of PVP; all approaches use ethylene glycol, PVP and Ag(NO)₃, and the AgNW dimensions are diameter (D) and length (L) and the ratio of PVP:Ag is given in terms of monomeric units.

aspect ratios.^{17,20} The details of the synthetic approaches and the results regarding the influence of PVP reported in the literature up to date are summarized in Table 1.

Unfortunately, PVP has the drawback of forming an insulating layer around the NW. This hinders tight AgNW contacts and decreases the conductivity of the AgNW network. To improve the AgNW electrode performance, post treatments like heating,²¹ low-temperature annealing,^{22,23} mechanical pressing,^{24,25} or chemical welding^{26,27} are necessary.

To the best of our knowledge, investigations on the influence of the average molar mass of PVP on the conductivity of a post-treated AgNW electrode do not exist in the literature. Therefore, after examining the PVP influence on the AgNW dimensions, we focus on investigating if the variation of the M_w of PVP has an impact on the conductivity of the transparent AgNW network after annealing.

Taking into account that the dimensions of the AgNWs correlate strongly with the resulting network conductivity,¹² the experiment can therefore only be accomplished with AgNWs of the same dimensions, but different PVP shells with regard to their M_w . Attempting to maintain the same dimensions of the AgNW network synthesized with PVPs with various M_w s, an extensive variation of the reaction temperature and reaction time was done in the frame of the present work.

Transparent electrodes were fabricated utilizing a large-scale spray coating process, followed by annealing and their conductivities were compared. Finally, the best performing electrode was incorporated into a small molecule organic solar cell to demonstrate its compatibility with typical processing technologies used in organic electronics.

Results and discussion

First, we synthesized AgNWs with comparable dimensions, but different PVP shells in order to further determine the influence of the average molar mass of PVP on the conductivity of the

AgNW network. A detailed overview of the obtained AgNW diameters and lengths is shown in Fig. 1. The values are plotted based on the M_w of PVP used in the respective segments for the reaction temperature and the corresponding reaction time. The colours represent the same reaction temperature and time. We utilized PVP with $M_w = 10$ kDa, 40 kDa, 55 kDa, 360 kDa or 1300 kDa, referred to as PVP10, PVP40, PVP55, PVP360 and PVP1300, respectively.

Temperature dependence in AgNW synthesis

In our experiments the polyol process was carried out varying the temperature between 135 and 150 °C and the reaction time between 5 and 2 h. To begin with, we compared the AgNW dimensions for performing the synthesis at 135 °C for 5 h (blue) or 140 °C for 4 h (orange). Concerning the PVP types, the diameter is approximately the same, except for PVP55, where it is larger by 73 nm at 140 °C and by 59 nm at 135 °C. The AgNWs are much longer when the reaction is performed at higher temperature. The exception here is PVP40, where the average length remained the same.

In order to obtain even thinner wires, we stopped the reaction at 140 °C after 2 h (green) and in all cases the diameter and the length decreased with a shorter reaction time. The length decrease was not as pronounced when PVP1300 was used. We also carried out the synthesis at 150 °C for 2 h (purple). In comparison to 140 °C for the same time, we observed a slight decrease of the diameter except for the synthesis with PVP40. Therein the average diameter decreased significantly from 112 nm to 61 nm. There is no pronounced trend between the AgNW lengths when comparing the reaction temperatures. Bergin *et al.* reported on the temperature effect on the AgNW diameter and length. They stated that a higher reaction temperature leads to an increased seed formation resulting in thinner and usually shorter NWs.¹² They also observed an increase of the diameter and length at a higher temperature, but the same reaction time and explained this with a faster reduction rate of EG at higher reaction temperatures.



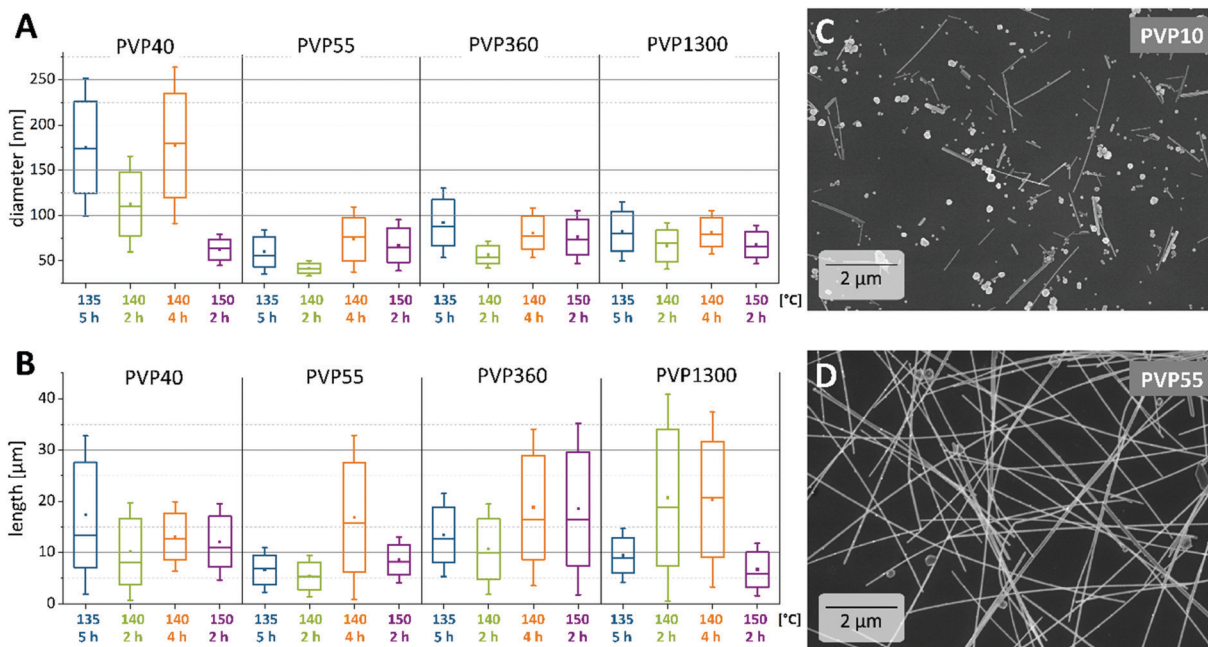


Fig. 1 (A) Diameters and (B) lengths of the AgNWs synthesized at different reaction temperatures, times and M_w of PVP. The corresponding colours in different frames reflect the same reaction temperature and time. (C) SEM images of the AgNWs synthesized at 140 °C for 2 h with (C) PVP10 or (D) PVP55.

Their findings are in accordance with our results with the exception that in our experiments the longest AgNWs grew at elevated temperatures (140 °C and 150 °C) instead of lower reaction temperatures. Possible reasons for the different results can be found in the slight deviation from the reaction procedure, *i.e.* the treatment of heated EG with a N_2 flow in our case as also described in an earlier study by Wiley *et al.*²⁸ Furthermore, the higher temperatures could accelerate the growth rate and led to longer AgNWs.

M_w of PVP dependence in AgNW synthesis

Next, the influence of the M_w of PVP is investigated. We, like previous studies, found the need of a minimum PVP chain length to successfully obtain AgNWs. In our procedure, the use of PVP10 leads to nanoparticles, nanorods and only a minor amount of nanowires (Fig. 1C). Even though AgNWs were produced with the capping agent PVP40, the as-synthesized AgNWs show a broad distribution in both diameter and length. Therefore, the minimum M_w required to synthesize AgNWs with a narrow diameter distribution was, in our case, 55 kDa (Fig. 1D). For the reactions carried out at 135 °C for 5 h (blue) and 140 °C for 2 h (green) or 4 h (orange), we could observe the same trend: the diameters of the NWs dropped from PVP40 to PVP55 and increased in the case of PVP360 or PVP1300. The diameter difference if PVP360 or PVP1300 was used was however marginal. Moreover, at a higher reaction temperature of 150 °C (purple) the diameter difference between the NWs synthesized with various M_w s of PVP was only in the range of 2–11 nm. With respect to the aspect ratio, we observed an increase of the aspect ratio if long chain PVP was utilized (Fig. 1A). The exception here is the synthesis at 150 °C for 2 h with PVP1300. Compared to PVP40 and PVP55,

the presence of PVP360 or PVP 1300 caused an increase in the aspect ratio. Being most pronounced at a reaction temperature of 140 °C for 2 h, the aspect ratio increased from 100 (PVP40) to 300 (PVP1300) (Fig. 1B). All together, we observed no distinct and unambiguous trends regarding the influence of the M_w of PVP on either the diameter or the aspect ratio across all reaction conditions. However, some tendencies can be obtained from the comparative analysis of our data and the literature reports, as discussed in the following. According to the simulations by Kyrychenko *et al.* reporting about the interactions between PVP of different chain lengths and Ag nanocrystals (NC), long-chain PVPs show a higher number of PVP-to-Ag contacts and a higher degree of polymer layers around the NC. These investigations could lead to an assumption that the diameters of the nanowires would decrease upon increasing the chain-length of PVP as a consequence of steric hindrance.²⁹ However, we observed a diameter decrease only when switching from PVP40 to PVP55. Utilizing PVP with longer chains (PVP360 and PVP1300) an opposite behavior occurs. To explain the diameter increase, we propose that the PVP chain length is decisive not only for governing the AgNW growth, but already during the nucleation of the Ag nanoparticles. Since the quantity of the pyrrolidone moieties remained constant, meaning that less numbers of polymer chains are present within the synthesis with respect to long-chain PVP, a fewer Ag nuclei (five-fold twinned decahedra) can be stabilized during the nucleation. This leaves more precursors per nuclei in the reaction mixture. Additionally, the higher viscosity of PVP360 and PVP1300 solutions in EG may reduce the nucleation rate. Our further understanding is that Ag atoms are preferentially added to an existing AgNW if they are in close spatial proximity. This is also probably the case for a coordinated Ag^+ at the carbonyl



group within the same polymer chain which is attached to the side of a growing AgNW in comparison to an Ag^+ at the adjacent carbonyl group elsewhere in the solution. Consequently, the longer the PVP chain, the more Ag^+ are present along the polymer chain to be added to an existing AgNW leading to an increase in diameter because of a higher degree of layering. The combination of these effects could result in AgNWs with enlarged diameters.

The increase of the aspect ratio with the M_w of PVP can be explained as follows: a longer polymer chain promotes the growth of AgNWs with high aspect ratios due to a greater number of contacts between Ag and long-chain PVP, as well as a higher degree of layering around the AgNW as mentioned before.²⁹ PVP1300 promoted the growth of AgNWs with a length up to 60 μm and PVP55 promoted the growth of a maximum of 10 μm long NWs (Fig. 2C and D). This could be due to the fact that a longer PVP chain leads to a better stabilization due to the higher number of contacts between the PVP and Ag. Furthermore, as mentioned above, a high number of Ag^+ coordinated at the longer polymer chain can readily attach at the ends of the existing AgNW rather than adding onto an adjacent one.

Altogether, the trends how the M_w of PVP affects the AgNW dimensions reported in the literature are sometimes contradictory. We suspected that the polydispersity of the commercially available PVP batches could be responsible for this. Indeed, size exclusion chromatography (SEC) revealed broad dispersities ($D = M_w/M_n$) higher than 3, meaning that the PVP powders are mixtures of strongly different chain lengths (Fig. S1, ESI[†]). This high polydispersity can explain the discrepancies in the influence of the M_w of PVP on the AgNW dimensions reported in both our work and in the above mentioned literature. Therefore, investigations of the used PVP are recommended and utilization of controlled

polymerized PVP owing to narrow dispersities may result in specified results. In general, there remains a lack of full understanding of the conformation, coil size, fluctuation, viscosity and influence of the polymer chain during the synthesis of AgNWs.

Role of PVP in the electrode performance

Despite repeated washing, it is generally known that a PVP layer remains around the AgNW. High resolution transmission microscopy (HR-TEM) revealed 1–4 nm thick shells around the AgNWs independent of the M_w of PVP. Fig. 3A exemplarily shows an AgNW with an amorphous PVP coating. At a higher magnification, the crystal properties can be evaluated with a lattice distance of 2.35 Å at the elongated side of the AgNW corresponding to the {100}-facet (Fig. 3B). However, the PVP shell is not clearly recognizable anymore.

As described above with variation of synthetic parameters such as temperature, reaction time and molar mass of PVP we produced AgNWs with average diameters from 41 to 137 nm and lengths from 3 to 20 μm . Since a comparison of the electrical performance is only possible with AgNWs of the same dimensions,¹² we chose AgNWs with nearly equal lengths from the plethora of synthesized AgNWs for the investigation of the influence of the M_w of PVP on the conductivity of the annealed AgNW networks. Herein, AgNWs with 60 nm and 80 nm diameters covered with PVP40, PVP55, PVP360 or PVP1300 were chosen as representative examples. Their diameter, length and corresponding aspect ratio are summarized in Table 2. The detailed information is found in Fig. S2 (ESI[†]). To distinguish the optimum annealing temperature, AgNWs were spray-coated onto glass substrates to reach a similar transmittance at 550 nm ($\%T_{550\text{nm}}$) of approximately 83% and the electrodes were then

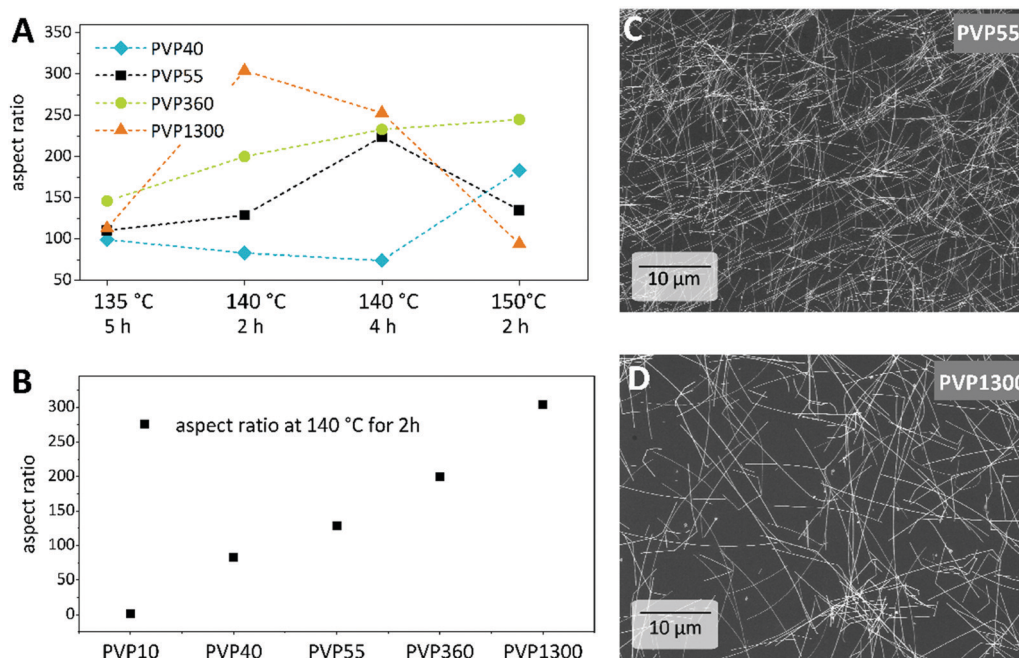


Fig. 2 Aspect ratios of the synthesized AgNWs with various M_w s of PVP obtained at (A) different reaction temperatures and times and (B) 140 °C for 2 h. SEM images of the AgNWs synthesized at 140 °C for 2 h in the presence of (C) PVP55 or (D) PVP1300.



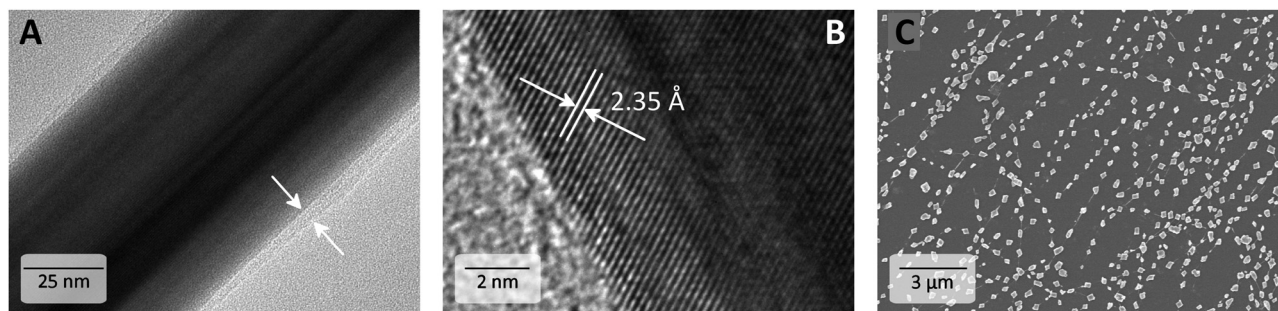


Fig. 3 (A) TEM image of a AgNW clearly shows a PVP shell, (B) HR-TEM image of a AgNW showing a lattice distance of 2.35 Å corresponding to the {100}-facet, and (C) SEM image of a destroyed AgNW network after gradual annealing until 250 °C.

Table 2 overview of the dimensions of AgNWs differing in the PVP shell used in heat treatment. The dimensions are diameter (D), length (L) and aspect ratio (A)

	AgNW60-PVP40	AgNW60-PVP55	AgNW60-PVP360	AgNW60-PVP1300	AgNW80-PVP55	AgNW80-PVP360	AgNW80-PVP1300
D [nm]	61 ± 12	64 ± 4	56 ± 10	66 ± 17	73 ± 24	81 ± 18	82 ± 21
L [μm]	12.0 ± 8.3	9.3 ± 6.8	10.6 ± 6.3	20 ± 14.2	16.9 ± 10.7	18.8 ± 10.1	9.4 ± 3.5
A	196	145	189	303	232	232	114

gradually heated from 75 °C to 250 °C on a hot plate for 20 min at each temperature. Between the heating steps the sheet resistance (R_s) was measured (R_s vs. T is shown in Fig. S3, ESI†). For all electrodes there are two distinguishable stages. First, the electrical resistance dropped until a minimum R_s was achieved with a heat treatment at 200 °C. After heating the electrodes to 225 °C, the conductivity diminished. The annealing steps are performed as follows: in the beginning, the PVP on the AgNW surface is partially desorbed, which improves the contact of the adjacent AgNWs and R_s decreased. At the glass temperature of PVP, *i.e.* 140–180 °C,^{30–33} the PVP shell softens and flows, further improving the junction contact. After an additional temperature increase, a partial degradation of PVP as well as local sintering at AgNW junctions due to diffusion enhances the electrical performance.³⁴ Further temperature elevation (225–250 °C) leads to coalescence of the unprotected AgNWs into disconnected droplets due to the Plateau-Rayleigh instability (Fig. 3C).³⁵ The latter is the decay of a cylindrical body into a particle chain driven by the instability caused by capillary force.

The driving force is the minimization of the surface energy. Hereby, mass transport occurs *via* surface diffusion and the volume is conserved during fragmentation. This behaviour was studied on thermally treated AgNWs,³⁵ copper nanowires,³⁶ and laser induced spheroidisation of metal films.³⁷ Also, Monte-Carlo simulations of thermal annealing of germanium nanowires predicted comparable fragmentations.³⁸

To gain an insight into the variances between the above mentioned electrodes, we measured the R_s at different % T . Hereby, after spray-coating only one annealing step was applied at an optimum annealing temperature of 200 °C for 20 min. The data were fitted using a model proposed by De *et al.*³⁹ to distinguish the performance in the percolative and bulk regime (Fig. 4A and B). High transmittance electrodes qualifying for optoelectronic device application are assigned to the percolative regime (80–99%). In the following the electrical performances of the AgNW60 and AgNW80 electrodes are compared to the same transmittance of 84% $T_{550\text{nm}}$. We found that AgNW60 electrodes performed the best if covered with shorter chain PVP as the

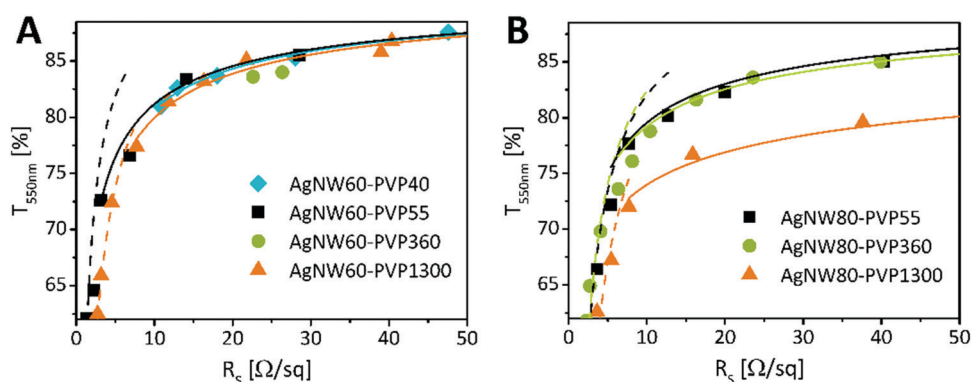


Fig. 4 Sheet resistance versus transmittance at 550 nm of AgNWs varying in the PVP-shell with (A) 60 nm and (B) 80 nm diameter. The dashed lines correspond to bulk behavior, and the continuous line corresponds to percolative behavior. Fitted with a model presented by De *et al.*³⁹



sheet resistances are $18 \Omega \text{ sq}^{-1}$ (PVP40) and $17 \Omega \text{ sq}^{-1}$ (PVP55). The resistances were higher if AgNW60 was covered with PVP360 ($26 \Omega \text{ sq}^{-1}$) or PVP1300 ($22 \Omega \text{ sq}^{-1}$). Regarding AgNW80, two systems performed equally well despite different PVP coatings: $R_s = 25 \Omega \text{ sq}^{-1}$ (PVP55) and $R_s = 28 \Omega \text{ sq}^{-1}$ (PVP360). Here, AgNW80 with PVP1300 showed the worst electrical performance with $90 \Omega \text{ sq}^{-1}$. We have to note that not only the PVP coverage can be taken into account to evaluate the performance of the electrodes. According to Bergin *et al.* the electrode transmittance increases with the nanowire length at a given sheet resistance which is due to the fact that less nanowire connections are necessary to achieve percolation.¹² Solely looking at the AgNW morphologies, a higher aspect ratio is expected to show better conductivity.¹⁷ Even though AgNW60–PVP1300 ($A = 303$) and AgNW60–PVP360 possess higher aspect ratios, it is outperformed by both AgNW60–PVP40 ($A = 196$) and AgNW60–PVP55 ($A = 145$). Regarding the performance of AgNW80, the influence of the M_w is not as strong as the impact of the aspect ratios of AgNW80–PVP55 and AgNW80–PVP360, which are the same ($A = 232$) and whose R_s differs slightly.

The lower electrical performance of AgNW80–PVP1300 can be explained by the more pronounced impact of the small aspect ratio of 114. The results show an inhibitory effect of long-chain PVP on the network conductivity for AgNW60 in spite of annealing. We suggest that the relatively lower influence of the M_w of PVP for AgNW80 can be attributed to the higher ratio of the AgNW diameter to the thickness of the PVP layer. We understand that for thicker NWs the contribution of the NW diameter to the final conductivity dominates over the influence of the PVP layer.

From these investigations, it can be concluded that the AgNW morphology and the aspect ratio play a fundamental role in the overall performance of the conductive networks. While the network conductivity for AgNW80 is not strongly affected by M_w , there is a negative impact of the higher M_w on the networks consisting of AgNW60. Therefore, preferentially shorter chain PVP should favor the synthesis of thin AgNWs with regard to well conducting networks. Utilizing thin or ultra-thin AgNWs is mainly desired for application in devices if low-haze electrodes are required, for instance in LEDs.⁸ Particularly, thin-film organic optoelectronic devices suffer from short circuits if AgNWs reach the upper layers.⁴⁰ The surface roughness of thin NWs is not as pronounced as compared to that of the thicker ones, which reduces the necessary amount of surface flatteners.⁴¹

Solar cell integration

To demonstrate the applicability of the investigated materials, the electrode AgNW60–PVP40 was integrated into an organic solar cell (OSC). Details such as a schematic layer stack, current density *versus* voltage (jV) characteristics and a summary of the electrode and photovoltaic performance can be found in the ESI† (Table S1 and Fig. S4). The AgNW electrode on glass is characterized by 85.5% transmittance at 550 nm and a sheet resistance of $24.4 \Omega \text{ sq}^{-1}$. In comparison, the ITO electrode shows $R_s = 30.4 \Omega \text{ sq}^{-1}$ at $80.8\%T_{550\text{nm}}$. The inherently rough AgNW network needs to be smoothed with an additional planarization layer. For this purpose, PEDOT:PSS is spin-coated directly on the structured AgNW electrode. Briefly, small molecule materials

DCV5T-Me and C_{60} are used as donor and acceptor molecules in a bulk heterojunction with n–i–p architecture, respectively.⁴² We show working OSCs with an efficiency of 2.4% on in-house synthesized and fabricated AgNW/PEDOT:PSS electrodes, comparable to a ITO/PEDOT:PSS reference device with an efficiency of 3.4%. In comparison to pristine ITO (PCE of 7.1%), the addition of PEDOT:PSS caused an decrease in efficiency. The utilized OSC layer stack is optimized for ITO and the AgNW based device performance could further be improved by adjusting the organic layers to the AgNW/PEDOT:PSS film thickness. Also, the AgNW electrodes exhibit a low specular reflection R_{vis} which does not support the microcavity effect.⁴³

Conclusions

We investigated the role of the average molar mass (M_w) of PVP in the polyol process in order to obtain AgNWs. By varying the reaction temperature and time as well as using PVP of different average molar masses, a variety of different AgNWs could be synthesized which differ in diameter and length. Subsequently, AgNW electrodes were fabricated with AgNWs of similar dimensions but different PVP shells. The AgNW dimensions control the main part on the network conductivity. Despite heat treatment we observed an inhibitory effect on the longer chain PVP for AgNWs with 60 nm diameter. This inhibition was not as pronounced for AgNWs with 80 nm diameter. Utilizing size exclusion chromatography, we determined that commercially available PVP batches were broadly distributed regarding the average molar mass. This can explain the diversity of the research results concerning the influence of the M_w of PVP on AgNW dimensions. The fabricated transparent electrodes showed a reasonably low sheet resistance of $R_s = 24.4 \Omega \text{ sq}^{-1}$ at $85.5\%T_{550\text{nm}}$ and can be incorporated in combination with PEDOT:PSS into a DCV5T-Me: C_{60} organic solar cell.

Experimental

Materials

The following chemicals and solvents were used to synthesize AgNWs. Silver nitrate (AgNO_3 , $\geq 99.9\%$) and poly(*N*-vinylpyrrolidone) (PVP, $M_w \approx 10\,000 \text{ g mol}^{-1}$ ($D = 3.5$), $40\,000 \text{ g mol}^{-1}$ (K30, $D = 3.9$), $55\,000 \text{ g mol}^{-1}$ ($D = 5.2$), $360\,000 \text{ g mol}^{-1}$ ($D = 4.8$)) were purchased from Sigma Aldrich; PVP with a $M_w \approx 1\,300\,000 \text{ g mol}^{-1}$ ($D = \text{N/A}$) was obtained from Alfa Aesar; iron(III) nitrate nonahydrate ($\text{Fe}(\text{NO}_3)_3 \cdot 9\text{H}_2\text{O}$, $\geq 90\%$) was obtained from Merck; PEDOT:PSS ‘PVP AI 4083’ (AI4083) was obtained from Heraeus Clevis, Germany; ethylene glycol ($\geq 99.0\%$) was obtained from J. T. Baker; sodium chloride (NaCl, 100%) and ethanol (absolute) were obtained from AnalaR NORMAPUR; and acetone (p.A.) was obtained from Fischer. Milli-Q[®]-water (Millipore) water was used.

Synthesis of silver nanowires

The synthesis of AgNWs was carried out based on a polyol approach reported by Bergin *et al.*¹² First, 39.6 ml ethylene glycol (EG) was added into a 100 ml flask and heated up to the



desired temperature in an oil bath. EG was kept at the set temperature for 1 h under constant agitation and purged with a nitrogen flow to remove water quickly. Meanwhile, four solutions were prepared: 0.1285 g NaCl in 10 ml EG (220 mmol l^{-1}), 0.0814 g $\text{Fe}(\text{NO}_3)_3$ in 10 ml EG (33 mmol l^{-1}), 0.2625 g PVP with desired M_w in 6.25 ml EG (378 mmol l^{-1}) and 0.2625 g AgNO_3 in 6.25 ml EG (247 mmol l^{-1}). After the nitrogen flow was stopped, the previously prepared solutions were added to the stirred EG in the following order with 30 s in between each addition: 50 μL NaCl in EG, 25 μL $\text{Fe}(\text{NO}_3)_3$ in EG, 5.19 ml PVP in EG and 5.19 ml AgNO_3 in EG. The mixture was allowed to react for a certain period of time without any agitation and cooled down to room temperature. Then it was equally divided into two centrifuge tubes, followed by an addition of 9 ml acetone and thorough vortexing. The AgNWs were collected upon centrifugation at 2000 rpm for 1 h. Afterwards, the supernatant was decanted until 5 ml was left and the centrifuge tube was filled up with water. After another centrifugation step, the obtained AgNWs were washed twice with ethanol (2000 rpm, 1 h) and redispersed in EtOH.

Electrode fabrication

Pre-cleaned and oxygen plasma treated (2×10^{-1} mbar, 10 min) BK7 glass substrates (Schott, Mainz, Germany) were used. Ethanolic dispersions of the synthesized AgNWs were sonicated for 2 min and then spray-coated using a nozzle (Fisnar, Wayne (NJ), USA) onto a heated substrate (80°C) with a spraying distance, a moving speed and a spraying pressure of the nozzle of 12 cm, 1.5 cm s^{-1} and 200 mbar, respectively.

Characterization

High resolution transmission electron microscopy (HR-TEM) was carried out using an FEI Tecnai F30 microscope operating at an accelerating voltage of 300 kV. Scanning electron microscopy (SEM) imaging was performed using a Zeiss DSM 982 Gemini instrument operating at 10 kV.

A four-point-probe setup (Lucas Labs, USA) was used for measuring the sheet resistances of the obtained electrodes. Optical characterization was carried out using an UV-VIS NIR photo spectrometer with an integrating sphere unit (Shimadzu, Japan). All transmission values are reported including the substrate transmission.

Conflicts of interest

The authors declare no competing financial interest.

Acknowledgements

This work was funded by the DFG Cluster of Excellence "Center for Advancing Electronics Dresden" (cfaed). We thank Susanne Goldberg for SEM measurements, Tobias Günther and Andreas Wendel for sample preparation, Sven Kunze and Andreas Büst for maintenance of the measurement systems, Thomas Gemming for providing support in HR-TEM imaging, and Donato Spoltore for discussions regarding the OSCs.

References

- W. Gaynor, S. Hofmann, M. G. Christoforo, C. Sachse, S. Mehra, A. Salleo, M. D. McGehee, M. C. Gather, B. Lüssem, L. Müller-Meskamp, P. Peumans and K. Leo, *Adv. Mater.*, 2013, **25**, 4006–4013.
- H.-G. Cheong, R. E. Triambulo, G.-H. Lee, I.-S. Yi and J.-W. Park, *ACS Appl. Mater. Interfaces*, 2014, **6**, 7846–7855.
- S. Cho, S. Kang, A. Pandya, R. Shanker, Z. Khan, Y. Lee, J. Park, S. L. Craig and H. Ko, *ACS Nano*, 2017, **11**, 4346–4357.
- J. Lee, P. Lee, H. Lee, D. Lee, S. S. Lee and S. H. Ko, *Nanoscale*, 2012, **4**, 6408–6414.
- Y. Park, L. Bormann, L. Müller-Meskamp, K. Vandewal and K. Leo, *Org. Electron.*, 2016, **36**, 68–72.
- F. Selzer, N. Weiß, D. Kneppel, L. Bormann, C. Sachse, N. Gaponik, A. Eychmüller, K. Leo and L. Müller-Meskamp, *Nanoscale*, 2015, **7**, 2777–2783.
- P. Zhang, I. Wyman, J. Hu, S. Lin, Z. Zhong, Y. Tu, Z. Huang and Y. Wei, *Mater. Sci. Eng., B*, 2017, **223**, 1–23.
- T. Sannicò, M. Lagrange, A. Cabos, C. Celle, J. P. Simonato and D. Bellet, *Small*, 2016, **12**, 6052–6075.
- D. Langley, G. Giusti, C. Mayousse, C. Celle, D. Bellet and J.-P. Simonato, *Nanotechnology*, 2013, **24**, 452001.
- B. Wiley, Y. Sun and Y. Xia, *Acc. Chem. Res.*, 2007, **40**, 1067–1076.
- N. Murshid and V. Kitaev, *Chem. Commun.*, 2014, **50**, 1247–1249.
- S. M. Bergin, Y.-H. Chen, A. R. Rathmell, P. Charbonneau, Z.-Y. Li and B. J. Wiley, *Nanoscale*, 2012, **4**, 1996–2004.
- M. Tsuji, Y. Nishizawa, K. Matsumoto, M. Kubokawa, N. Miyamae and T. Tsuji, *Mater. Lett.*, 2006, **60**, 834–838.
- X. Zeng, B. Zhou, Y. Gao, C. Wang, S. Li, C. Y. Yeung and W. Wen, *Nanotechnology*, 2014, **25**, 495601.
- J.-J. Zhu, C.-X. Kan, J.-G. Wan, M. Han and G.-H. Wang, *J. Nanomater.*, 2011, **2011**, 1–7.
- B. Li, S. Ye, I. E. Stewart, S. Alvarez and B. J. Wiley, *Nano Lett.*, 2015, **15**, 6722–6726.
- Q. Xue, W. Yao, J. Liu, Q. Tian, L. Liu, M. Li, Q. Lu, R. Peng and W. Wu, *Nanoscale Res. Lett.*, 2017, **12**, 480.
- N. de Guzman and M. D. L. Balela, *J. Nanomater.*, 2017, **2017**, 1–14.
- Y.-J. Song, M. Wang, X.-Y. Zhang, J.-Y. Wu and T. Zhang, *Nanoscale Res. Lett.*, 2014, **9**, 17.
- Y. Ran, W. He, K. Wang, S. Ji and C. Ye, *Chem. Commun.*, 2014, **50**, 14877–14880.
- Y. Jia, C. Chen, D. Jia, S. Li, S. Ji and C. Ye, *ACS Appl. Mater. Interfaces*, 2016, **8**, 9865–9871.
- N. Weiß, L. Müller-Meskamp, F. Selzer, L. Bormann, A. Eychmüller, K. Leo and N. Gaponik, *RSC Adv.*, 2015, **5**, 19659–19665.
- F. Selzer, N. Weiß, L. Bormann, C. Sachse, N. Gaponik, L. Müller-Meskamp, A. Eychmüller and K. Leo, *Org. Electron.*, 2014, **15**, 3818–3824.
- T. Tokuno, M. Nogi, M. Karakawa, J. Jiu, T. T. Nge, Y. Aso and K. Suganuma, *Nano Res.*, 2011, **4**, 1215–1222.
- J. H. Seo, I. Hwang, H.-D. Um, S. Lee, K. Lee, J. Park, H. Shin, T.-H. Kwon, S. J. Kang and K. Seo, *Adv. Mater.*, 2017, **29**, 1701479.
- Y. Ge, X. Duan, M. Zhang, L. Mei, J. Hu, W. Hu and X. Duan, *J. Am. Chem. Soc.*, 2018, **140**, 193–199.



- 27 F. Xu, W. Xu, B. Mao, W. Shen, Y. Yu, R. Tan and W. Song, *J. Colloid Interface Sci.*, 2018, **512**, 208–218.
- 28 B. Wiley, Y. Sun and Y. Xia, *Langmuir*, 2005, **21**, 8077–8080.
- 29 A. Kyrychenko, O. M. Korsun, I. I. Gubin, S. M. Kovalenko and O. N. Kalugin, *J. Phys. Chem. C*, 2015, **119**, 7888–7899.
- 30 M. del, P. Buera, G. Levi and M. Karel, *Biotechnol. Prog.*, 1992, **8**, 144–148.
- 31 B. C. Hancock and G. Zografi, *Pharm. Res.*, 1994, **11**, 471–477.
- 32 R. Nair, N. Nyamweya, S. Gönen, L. J. Martínez-Miranda and S. W. Hoag, *Int. J. Pharm.*, 2001, **225**, 83–96.
- 33 S. Vijaykumar, S. Prasannkumar, B. S. Sherigara, N. B. Shelke, T. M. Aminabhavi and B. S. R. Reddy, *Macromol. Res.*, 2009, **17**, 1003–1009.
- 34 M. Lagrange, D. P. Langley, G. Giusti, C. Jiménez, Y. Bréchet and D. Bellet, *Nanoscale*, 2015, **7**, 17410–17423.
- 35 D. P. Langley, M. Lagrange, G. Giusti, C. Jiménez, Y. Bréchet, N. D. Nguyen and D. Bellet, *Nanoscale*, 2014, **6**, 13535–13543.
- 36 M. E. Toimil Molares, A. G. Balogh, T. W. Cornelius, R. Neumann and C. Trautmann, *Appl. Phys. Lett.*, 2004, **85**, 5337–5339.
- 37 F. Ruffino and M. G. Grimaldi, *Phys. Status Solidi*, 2015, **212**, 1662–1684.
- 38 T. Müller, K.-H. Heinig and B. Schmidt, *Mater. Sci. Eng., C*, 2002, **19**, 209–213.
- 39 S. De, P. J. King, P. E. Lyons, U. Khan and J. N. Coleman, *ACS Nano*, 2010, **4**, 7064–7072.
- 40 H. Wang, K. Li, Y. Tao, J. Li, Y. Li, L.-L. Gao, G.-Y. Jin and Y. Duan, *Nanoscale Res. Lett.*, 2017, **12**, 77.
- 41 W. Gaynor, G. F. Burkhard, M. D. McGehee and P. Peumans, *Adv. Mater.*, 2011, **23**, 2905–2910.
- 42 R. Meerheim, C. Körner and K. Leo, *Appl. Phys. Lett.*, 2014, **105**, 063306.
- 43 L. Bormann, F. Nehm, L. Sonntag, F.-Y. Chen, F. Selzer, L. Müller-Meskamp, A. Eychmüller and K. Leo, *ACS Appl. Mater. Interfaces*, 2016, **8**, 14709–14716.

